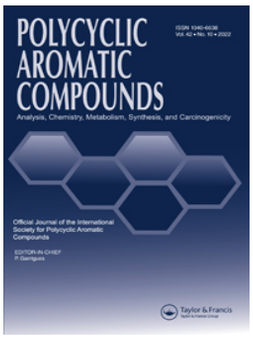

Polycyclic Aromatic Compounds

ISSN: (Print) (Online) Journal homepage: https://www.tandfonline.com/loi/gpol20

Quantum Chemical Calculations of 5-Diethylamino-2-{[4-(3-Methyl-3-Phenyl-Cyclobutyl)-Thiazol-2-yl]-Hydrazonomethyl}-Phenol Single Crystal Containing Heteroatoms

Tuncay Karakurt, Muharrem Dinçer, Alaaddin Cukurovali & Ibrahim Yilmaz

To cite this article: Tuncay Karakurt, Muharrem Dinçer, Alaaddin Cukurovali & Ibrahim Yilmaz (2022) Quantum Chemical Calculations of 5-Diethylamino-2-{[4-(3-Methyl-3-Phenyl-Cyclobutyl)-Thiazol-2-yl]-Hydrazonomethyl}-Phenol Single Crystal Containing Heteroatoms, Polycyclic Aromatic Compounds, 42:10, 7476-7499, DOI: 10.1080/10406638.2021.2004173

To link to this article: https://doi.org/10.1080/10406638.2021.2004173

Published online: 18 Nov 2021.

POLYCYCLIC AROMATIC COMPOUNDS
2022, VOL. 42, NO. 10, 7476–7499
https://doi.org/10.1080/10406638.2021.2004173

Taylor & Francis
Taylor & Francis Group

Quantum Chemical Calculations of 5-Diethylamino-2-{[4-(3-Methyl-3-Phenyl-Cyclobutyl)-Thiazol-2-yl]-Hydrazonomethyl}-Phenol Single Crystal Containing Heteroatoms

Tuncay Karakurt[a], Muharrem Dinçer[b], Alaaddin Cukurovali[c], and Ibrahim Yilmaz[d]

[a]Department of Chemical Engineering, Faculty of Engineering-Architecture, Kirsehir Ahi Evran University, Kirsehir, Turkey; [b]Department of Physics, Faculty of Arts and Sciences, Ondokuz Mayis University, Kurupelit, Samsun, Turkey; [c]Department of Chemistry, Faculty of Science, Firat University, Elazig, Turkey; [d]Department of Chemistry, Kamil Ozdag Science Faculty, Karamanoglu Mehmetbey University, Karaman, Turkey

ABSTRACT

5-Diethylamino-2-{[4-(3-methyl-3-phenyl-cyclobutyl)-thiazol-2-yl]-hydrazonomethyl}-phenol single crystal was synthesized and by using FT-IR, NMR and UV-Vis spectral techniques and X–ray diffraction method were characterized. It has adopted an enol-imine tautomeric form with a strong intramolecular O–H···N and intermolecular N–H···N hydrogen bond interaction. The compound has a photochromic property and is not planar. NMR chemical shift values, FT-IR and UV-Vis spectra of the title compound were theoretically calculated using density functional theory (DFT) and the spatial magnetic property known as visual ICSS employing the NICS concept was calculated. Using the TD–DFT method, the electronic absorption spectrum was calculated and determined to be in good agreement with the experimental UV–Vis values. It has been found that the title compound may have two tautomer structures (enol-imine and keto-amine). Tautomeric structures of the title compound were used to investigate corrosion inhibition effect on Cu and Fe metal atoms. Some quantum chemical parameters such as HOMO and LUMO orbital energies, electron affinity (IE), ionization potential (EA), electronegativity (χ), global hardness (η) and global softness (S) were calculated. Using these parameters, the fraction of electrons (δ) transfer from inhibitor to metal was calculated to investigate the corrosion inhibition effects of Cu and Fe metals of the two tautomer structures. The corrosion inhibition effects of these structures were compared with the help of calculated quantum chemical parameters, and the relationships between quantum chemical parameters and the corrosion inhibition mechanism were analyzed. Electrophilic and nucleophilic attack sites of these tautomers also were examined using Fukui functions. In addition, optimized structure of the title compound in the solid phase was obtained using *Quantum ESPRESSO* under periodic boundary conditions (PBC).

ARTICLE HISTORY
Received 15 April 2020
Accepted 27 October 2021

KEYWORDS
FT-IR; NMR and UV–Vis spectral techniques; X-ray; ICSS; corrosion inhibition; electrophilic and nucleophilic attack

1. Introduction

Schiff bases, especially o-hydroxy derivatives, are donor compounds with unique structural and electronic properties for the preparation of biofunctional compounds,[1] molecular switches[2] and

CONTACT Tuncay Karakurt tuncaykarakurt@gmail.com Department of Chemical Engineering, Faculty of Engineering-Architecture, Kirsehir Ahi Evran University, Kirsehir 40100, Turkey.

optoelectronic materials.[3] These structures can exist as different tautomers. Tautomeric structures are very important in an area such as pharmacy, which they can be recognized by biological systems. The presence of a tautomer in solution has been shown to depend on factors that affect the equilibrium ratio of various parameters such as temperature, concentration, pH and solvent, while only one of the tautomers is observed in the solid state.[4] Schiff bases prepared by the reaction of salicylaldehydes, this mutual conversion between enol-imine and keto-amine tautomers, formed by intramolecular hydrogen migration caused by light absorption or temperature change, enables the molecule to display photochromism (enol-imine) and thermochromism (keto-amine) characteristics. Schiff bases containing substituted salicylaldehydes also have multiple enhanced biological activity.[5–8] Corrosion is the process of degradation of metallic materials by interacting with the components of the environment through chemical and/or electrochemical reactions. It causes great economic and security losses.[9–11] The economies of both developed and developing countries are badly affected by the damage caused by corrosion.[12] Aluminum and its alloys are of great interest in engineering applications due to their low cost, light weight, high thermal and electrical conductivity. In addition, aluminum has found wide use in corrosion environments, including the oil and gas industries.[13] The reliability, performance and safety of a wide variety of engineering systems depend on corrosion protection. The use of corrosion inhibitors and protective coatings are among the different corrosion protection approaches.[14–16] Aluminum and its alloys have corrosion resistance to a wide range of corrosive environments due to the development of a protective, tightly bonded passive layer on its surface. It is very practical to add corrosion inhibitors to reduce the corrosion rate of aluminum. The prevention of corrosion of aluminum and its alloys by organic inhibitors has been extensively studied in the literature.[17] The corrosion inhibitors used can be organic or inorganic chemicals added in small concentrations to solutions. Organic inhibitor molecules act by adsorption on the metal surface by forming a protective layer.[18] Organic compounds containing functional electronegative groups in triple and conjugated double bonds have been widely accepted as effective corrosion inhibitors. The inhibitory effect of an organic compound is reinforced by the presence of heteroatoms such as sulfur (S), nitrogen (N) and oxygen (O), which have an adsorption effect in its structure.[19,20] Experimental tools are useful in explaining the corrosion inhibition mechanism, but since they are expensive and time consuming, corrosion inhibition research have made significant progress using theoretical computational chemistry methods.[21]

In this study, the molecular structure of a new Schiff-based compound was determined by X-ray diffraction studies and comparisons were made with similar molecules in the literature. At the same time, FT-IR, NMR and UV-Vis spectroscopic studies of the title molecule were carried out to support results obtained by X-ray structure analysis. Theoretical calculations of molecular geometries, FT-IR, NMR and UV-Vis spectra were also performed to support experimental studies. The dependence of inhibition activity on quantum chemical descriptors such as E_{HOMO}, E_{LUMO}, global softness (S), Ionization potential (IP), Electron affinity (EA), absolute electronegativity (χ), indices for local nucleophilic (f_k^+) and electrophilic attacks (f_k^-) and local softness (S^+ and S–) has also been investigated on two tautomer structures.

2. Materials and methods

2.1. Computational details

For Molecular Modeling, the initial structure of the title compound was obtained from X-ray coordinates. For all theoretical calculations, Becke's three-parameter hybrid exchange functionals (B3)[22] using the Lee–Yang–Parr (LYP)[23] correlation functionals with the 6–31 G (d, p) basis set[24] were used by using Gaussian 09 software package[25] and the output files were analyzed by visual inspection with the GaussView molecular visualization program.[26] The vibration frequencies,

which scaled with 0.9613, and ^{1}H-^{13}C NMR chemical shifts in the GIAO approach were calculated on the optimized structure of the compound using the IEF–PCM (Integral–Equation–Formalism Polarizable Continuum Model)[27] model. In order to define the proton transfer and its potential barrier height between the O1 and N3 atoms in the molecule, by changing the O1-H1 bond length from 0.98 to 1.80 Å with 18 steps of 0.05 Å, the Potential Energy Surface (PES) scan was performed on the optimized geometry of the tautomeric form with AM1 method.[28] Electronic absorption spectra were calculated in chloroform solution using time dependent density functional theory (TD-DFT) method. The Fukui functions were calculated using the Multiwfn software[29] with the use of the energy output file from Gaussian 09. The solid phase calculations were performed under the generalized gradient approach (GGA) and Perdew-Burke-Ernzerhof (PBE)[30] pseudo potentials using the Quantum Espresso[31] software which use the density functional theory (DFT).

2.2. Synthesis

The title compound was synthesized according to the procedure in Scheme 2. 4-Diethylamino-2-hydroxy-benzaldehyde (10 mmol, 1.9324 g) was added to thiosemicarbazide (10 mmol, 0.9114 g) in 50 ml of ethanol and stirred at room temperature. Subsequently, a solvent of 1-methyl-1-phenyl-3-(2-chloro-1-oxoethyl) cyclobutane (α-haloketone) (2.2271 g, 10 mmol) in 20 ml of pure ethanol was added and the temperature was raised to 323–328 K and allowed to stand for 2 hours. The solution was then allowed to cool to room temperature. After cooling, it was made basic with an aqueous solution of NH_3 (5%), and the single crystals suitable for X-rays were obtained by washing several more times with an aqueous solution of NH_3, followed by drying. Yield: 67%, melting point: 431 K (Figure 1). Characteristic IR bands: ν(–OH) stretching band is invisible in the FT-IR spectra of the compound, 3120 cm^{-1} ν(N–H), 2973–2858 ν (aliphatics), 1634 cm^{-1} ν(C = N carbazone), 1596 cm^{-1} ν(C = N thiazole), 1131 ν(C–O), 701 cm^{-1} ν(C–S–C thiazole). Characteristic ^{1}H NMR shifts ($CDCl_3$, δ, ppm): 1.18 (t, j = 7.04 Hz, 6H, -CH_3s on aniline group), 1.50 (s, 3H, -CH_3 on cyclobutane), 2.49 (d, j = 9.88 Hz, 4H, -CH_2-, in cyclobutane ring), 3.36 (q, j = 7.04 Hz, 4H, -CH_2-, on aniline group), 3.56 (quintet, j = 7.8 Hz, 1H, >CH- in cyclobutane ring), 6.05 (s, 1H, =CH-S, in thiazole ring), 6.20-6.24 (m, 2H, aromatics), 6.96 (d, j = 8.66 Hz, 1H, aromatics), 7.10–7.20 (m, 3H, aromatics plus –NH-), 7.26-7.32 (q, j = 7.65 Hz, 3H, aromatics), 7.96 (s, 1H, =CH-S, azomethine), 10.67 (brs, 1H, -OH). Characteristic ^{13}C NMR shifts ($CDCl_3$, δ, ppm): 168.62, 159.70, 152.29, 151.94, 150.21, 148.27, 131.66, 128.27, 125.43, 124.67, 106.81, 103.76, 99.32, 98.26, 44.51, 40.05, 38.92, 30.11, 30.00, 12.67.

2.3. X-ray crystallography

At room temperature (296 K), diffraction measurements were performed for a suitable single crystal sample which has dimensions 0.42 × 0.24 × 0.08 mm with graphite monochrome Mo-Kα (λ = 0.71073 Å) radiation and a STOE IPDS 2 diffractometer. The structure was solved by direct methods using SHELXT-2015.[32] The refinement process was carried out anisotropically in the next stage of the isotropic positions of atoms other than hydrogen atom. The atomic positions of the hydrogen atoms belonging to the OH group was found from the difference Fourier map,

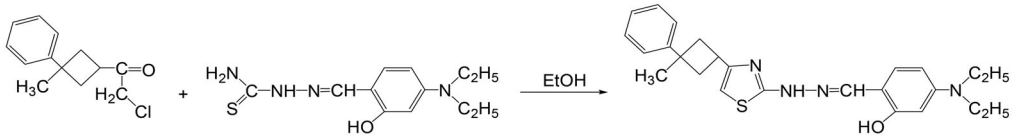

Figure 1. Synthetic route for the synthesis of the target compound.

Table 1. Crystallographic data for title compound.

Empirical formula	$C_{25}H_{30}N_4OS$
Formula weight	434.59
Temperature (K)	293(2)
Crystal system	monoclinic
Space group	$P2_1/c$
a (Å)	7.3563(5)
b (Å)	28.6840(15)
c (Å)	12.3687(7)
α (°)	90
β (°)	116.799(5)
γ (°)	90
Volume (Å^3)	2329.6(3)
Z	4
ρ_{calc} (g/cm^3)	1.239
μ (mm^{-1})	0.163
F(000)	928.0
Crystal size (mm^3)	0.42 × 0.24 × 0.08
Radiation	Mo-Kα ($\lambda = 0.71073$)
2Θ range for data collection (°)	3.954 to 53.498
Index ranges	$-9 \le h \le 9$, $-36 \le k \le 36$, $-15 \le l \le 15$
Reflections collected	18,227
Independent reflections	4940 [R_{int}= 0.0625, R_{sigma}= 0.0725]
Reflections observed [$I \ge 2\sigma(I)$]	2193
Data/restraints/parameters	4940/0/377
Goodness-of-fit on F^2	0.872
Final R indexes [$I \ge 2\sigma$ (I)]	R_1= 0.0508, wR_2= 0.1096
Final R indexes [all data]	R_1= 0.1369, wR_2= 0.1359
Largest diff. peak/hole (e Å^{-3})	0.30/–0.30
CCDC	885164

while those of all other hydrogen atoms were determined geometrically. The bond distances were fixed to 0.930 Å [Uiso(H) = 1.2 Ueq(C)], 0.860 Å [Uiso(H) = 1.5 Ueq(O)], 0.960 Å [Uiso(H) = 1.5 Ueq(C)] and 0.970 Å [Uiso(H) = 1.2 Ueq(C)] for the groups CH, NH, CH_3 and CH_2, respectively using a riding model. In structure refinement, 284 parameter differences used to refine by Fourier method considering 2193 reflections that meet the condition of $I > 2\sigma(I)$ from 4940 independent reflections measured using SHELXL-2015.[33] In the end of refinement process, R1, wR2 and S values of the title crystal were found to be 0.0532, 0.1221 and 0.876, respectively. The plots were generated by using Olex2[34] software. The conditions and parameters of the data collection process are listed in Table 1.

3. Results and discussion

3.1. Geometrical structure

An Ortep-3 view shown in Figure 2 crystallizes in the monoclinic space group P21/c, which is four molecules per unit cell.

The title molecule comprises a cyclobutane A(C8-C11), a thiazole B(N1/C14/S1/C13/C12), a benzene C (C1-C6) and a phenol D (C16-C21/O1) rings. The dihedral angles between rings are 54.3(2)° (AIB), 42.8(3)° (AIC), 52.0(2)° (AID), 89.54(18)° (BIC), 8.93(15)° (BID) and 89.27(18)° (CID).

Experimental and calculated bond lengths, bond angles, and torsion angles are also shown in Table 2. The bond lengths of C8-C9, C10-C11, C1-C6, N2-N3, N2-C14, C15-N3, S1-C13, C14-S1, C14 = N1, and C21-O1 of the title compound were experimentally 1.551(4), 1.547(4), 1.381(5), 1.381(3), 1.310(3), 1.282(3), 1.725(4), 1.745(3), 1.341(4) and 1.355(3) Å respectively, which is lengths are in literature values; 1.550(3), 1.548(3), 1.381(3), 1.379(2), 1.364(3), 1.275(3), 1.734(2), 1.728(2) and 1.364(3)[35] and 1.351(3) Å.[36] In the gas phase, these bond lengths have been

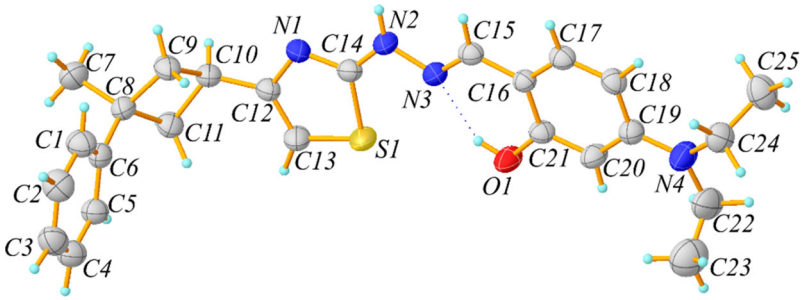

Figure 2. The experimental geometric structure of the title compound.

calculated as 11.564, 1.401, 1.401, 1.357, 1.368, 1.296, 1.753, 1.761, 1.303 and 1.350 Å and 1.565, 1.559, 1.401, 1.348, 1.372, 1.290, 1.752, 1.758[35] and 1.345 Å[36] in the literature.

The C21–O1 and C16–C15 bonds with single bond character and C21–C16 and C15– N3 bonds with double bond character prove that the title compound adopts the enol-imine tautomer. Based on these results, we can say that the compound is not planar and exhibits photochromic properties.[37]

A common feature of the enol-imine systems is that there is a strong intramolecular hydrogen bond between the N and O atoms.[38,39] Similarly, a strong intramolecular hydrogen bond was formed in the title crystal and the N3 … O1 distance is 2.650 (3) Å and characterized by an S(6) motif. The title molecule is stabilized by one intramolecular O1–H1A … N3 and one intermolecular N2–H2A··· N1 (symmetry code; (i) -x, -y, -z) which characterized an motif (Figure 3). The atom C25 at (x, y, z) forms C25–H25A···Cg3 (π-ring) contact, this time via atom H25, with the centroid of the C1-C6 ring [fractional centroid coordinates: 0.0439(2), 0.22928(6), 0.35177(14)] of the molecule at (1 – x, –1/2 + y, 1/2 – z) (Figure 4). In addition, within the title compound, there is a $\pi\pi$ interactions occur between the thiazole and phenol rings of neighboring molecules linked by symmetry. The centroid–centroid distance between Cg2 (B ring) and Cg4 (D ring) [symmetry code: –1 + x, y, z] is 3.714(18) Å (Figure 4) and details are given in Table 3. The cyclobutane ring is non-planar and is puckered due to its steric effect. This puckering forms a dihedral angle of 19.48 (14)° between the planes formed by the C9/C8/C11 and C11/C10/C9 atoms. This value is smaller than in the previously published literature; 21.3 (8)°.[40] There are three bond lengths that characterize the thiazole ring. These are bond distances of C12–N1 (1.396 (3) Å) with single bond character and C12–C13 (1.345 (3) Å) and N1–C14 (1.340 (4) Å) with double bond character. The bond lengths S1–C13 and S1–C14 are shorter than the accepted value for an S–Csp2 single bond (1.76 Å[41]) because they result from the conjugation of the electrons of the S1 atom with the C13 and C14 atoms.

3.2. Theoretical structures

PES analysis was performed using the AM1 method to determine all possible conformations of enol-imine and keto-amine forms in gas phase. As shown in Figure 5, the conformations corresponding to local and global minimum points obtained by PES analysis were optimized using the B3LYP/6-31G(d, p) level with the Gaussian 09 package program. As a result of these calculations, the lowest energy stable structures of both structures were obtained (Figure 6). However, as a result of the calculations, the values of the root mean square error (RMSE) of the bond lengths were found to be approximately 0.058 Å for the B3LYP and 0.022 Å for the GGA method and 1.155 and 1.029 Å for the bond angles, respectively for enol-imine form. This showed that bond lengths and angles obtained by GGA method had the strongest correlation with experimental values. Experimental and calculated other selected geometric parameters are listed in Table 2.

Table 2. Selected experimental and calculated geometric parameters.

Parameters	Experimental	B3LYP/6–31G(d,p) gas phase	GGA solid phase
Bond lengths (Å)			
C24–N4	1.466(4)	1.460	1.463
N4–C19	1.366(4)	1.381	1.374
N4–C22	1.531(5)	1.461	1.461
C15–N3	1.282(3)	1.296	1.309
C21–O1	1.355(3)	1.350	1.360
N3–N2	1.381(3)	1.357	1.363
N2–C14	1.310(3)	1.368	1.367
C14–N1	1.341(4)	1.303	1.323
C14–S1	1.745(3)	1.761	1.749
N1–C12	1.397(3)	1.388	1.393
C2–C1	1.377(4)	1.395	1.395
C1–C6	1.381(5)	1.401	1.404
S1–C13	1.725(4)	1.753	1.731
C9–C10	1.551(4)	1.559	1.563
C9–C8	1.551(4)	1.564	1.567
C8–C11	1.552(4)	1.564	1.562
C10–C11	1.547(4)	1.401	1.550
C6–C5	1.381(4)	1.549	1.401
C12–C13	1.345(4)	1.363	1.370
C12–C10	1.480(4)	1.497	1.498
C20–C21	1.370(4)	1.392	1.390
C15-C16	1.439(4)	1.442	1.438
RMSE[a]		0.055	0.022
Bond angles (°)			
C6–C1–C2	121.6(4)	121.0	121.1
C8–C9–C10	90.3(2)	88.9	89.9
C13–S1–C14	89.94(15)	87.4	88.5
N1–C12–C13	113.2(3)	115.5	115.2
C17–C18–C19	120.0(3)	120.3	120.4
C19–N4–C24	123.1(3)	121.9	122.8
C19–N4–C22	120.5(3)	121.8	121.6
N4–C19–C20	121.9(3)	121.3	120.9
N3–C15–C16	123.1(2)	122.9	122.6
O1–C21–C20	118.0(2)	117.1	118.6
O1–C21–C16	121.2(2)	122.1	120.2
C15–N3–N2	112.7(2)	118.3	119.2
RMSE[a]		1.155	1.029
Torsion angles (°)			
C25–C24–N4–C19	−92.3(5)	−90.9	−97.3
C25–C24–N4–C22	85.7(5)	91.6	83.9
C19–C18–C17–C16	0.4(5)	−0.2	0.78
C19–C20–C21–O1	−179.0(3)	−179.5	−178.8
N1–C14–N2–N3	179.6(3)	−177.7	174.3
C12–C13–S1–C14	−0.2(3)	0.0	−0.23

Since a single isolated molecule that does not interact with neighboring molecules in the gas phase is used, deviations from the experimental data occurred in the calculations. The GGA method, on the other hand, is the calculation made in the crystal phase and since the interactions of molecules in the unit cell with each other are taken into account, it is more compatible with the experimental results.

In addition, the total lattice energy values per unit cell were obtained by using the scf (self-consistent field) method and GGA exchange-correlation of both forms. As a result of the calculation, the lattice energy values of the enol-imine and keto-amine forms (Figure 7) were calculated as −1913.48332491 and −1913.37844988 Ry, respectively. This situation showed that the enol-

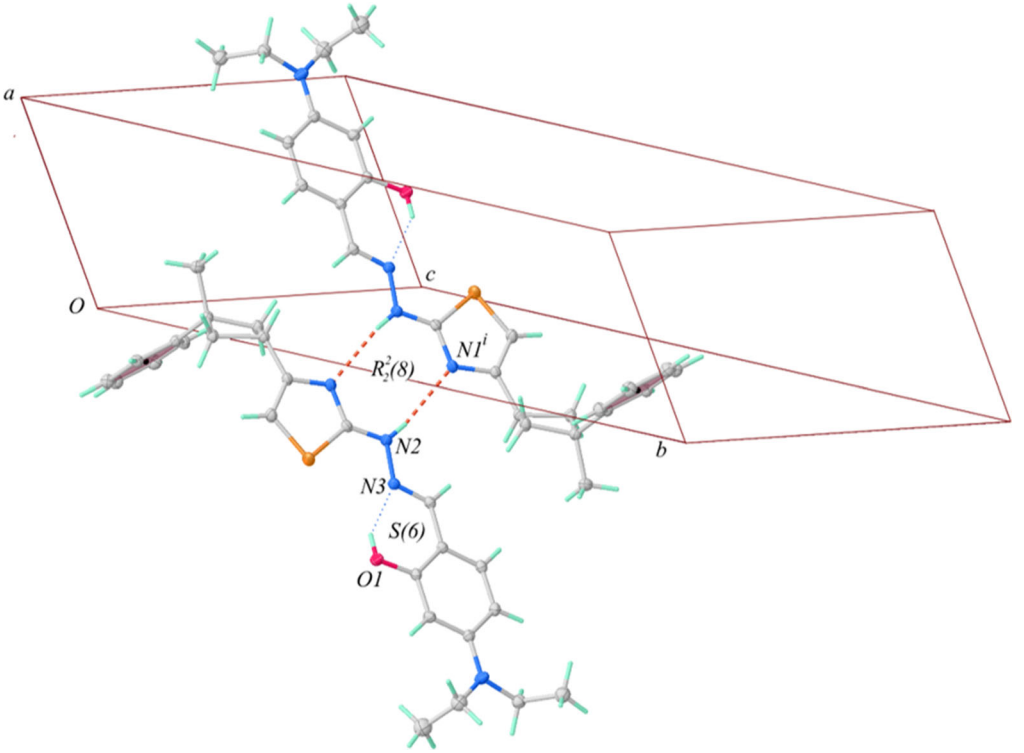

Figure 3. Part of the crystal structure of the title molecule, showing the formation of a motif $R_2^2(8)$ dimers.

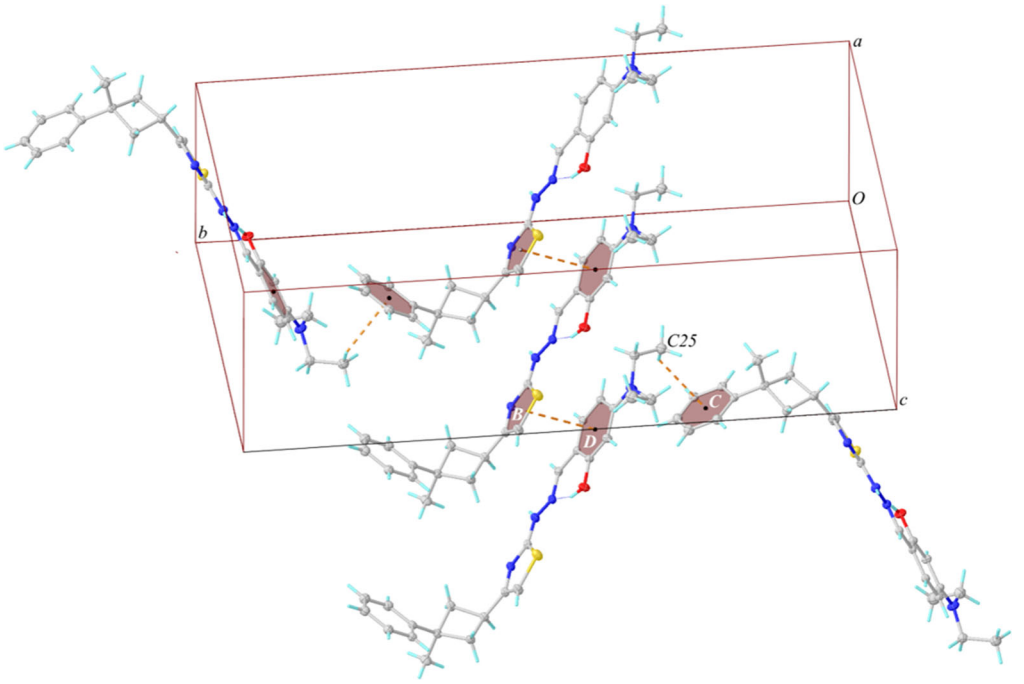

Figure 4. Packing of the title crystal with C–H π and π–π interactions along the c axis.

Table 3. Hydrogen bonding geometry (Å, °) for the title compound.

	D–HA	D–H	HA	DA	D–HA
X-ray	O1–H1A···N3	0.83(4)	1.93(4)	2.650(3)	146(4)
	N2–H2A···N1^{i}	0.86	2.24	3.034(3)	153
	C25–H25B···*Cg3*^{ii}	0.96	2.94(6)	3.538(6)	119(3)
	Cg(I)	Cg(J)	**Cg···Cg (Å)**		
	Cg2	Cg4^{iii}	3.714(18)		
Gas phase	O1–H1···N3	0.987	1.819	2.683	144
	N2–H2···N1	1.050	1.873	2.918	173
Solid phase	O1–H1 … N3	1.005	1.730	2.647	149
	N2–H2···N1	1.040	2.131	3.160	169

Symmetry codes: (i) *–x, –y, –z;* (ii) 1 – *x*, –1/2 + *y*, 1/2-*z*; (iii) –1 + *x*, *y*, *z* Cg2:S1/C13/C12/N1-C14 ring center; Cg3:C1–C6 ring center; Cg4:C16– C21 ring center.

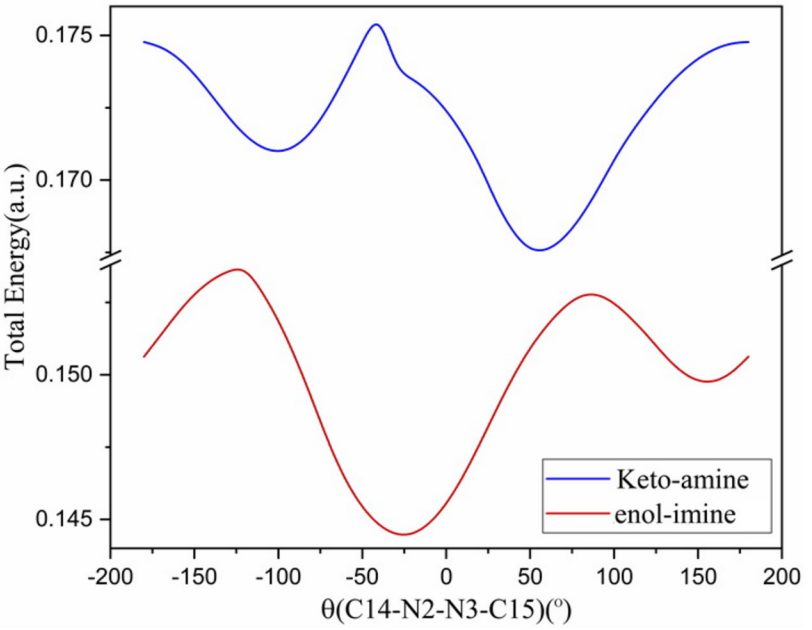

Figure 5. Molecular energy profile versus the selected torsional degree of freedom.

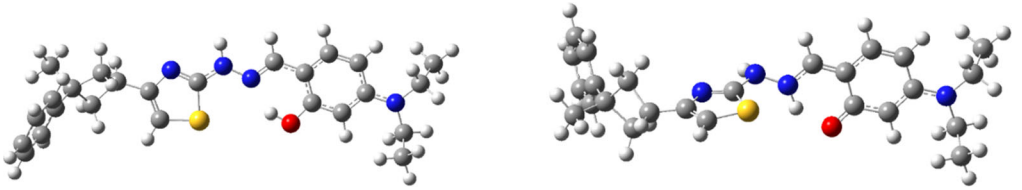

Figure 6. Optimize structures a) enol-imine b) keto-amine of the title compound.

imine form has a more stable structure than the keto-amine form in the calculations made in the crystal phase.

For the two tautomers (enol-imine and keto-amine), which the crystal can be present, the potential barrier to the process of proton transfer in the molecule was calculated by PES analysis (Figure 8). The AM1 method was used for this calculation and the enol-imine form was found to be more stable than the keto-amine form. The energy difference between the two tautomeric

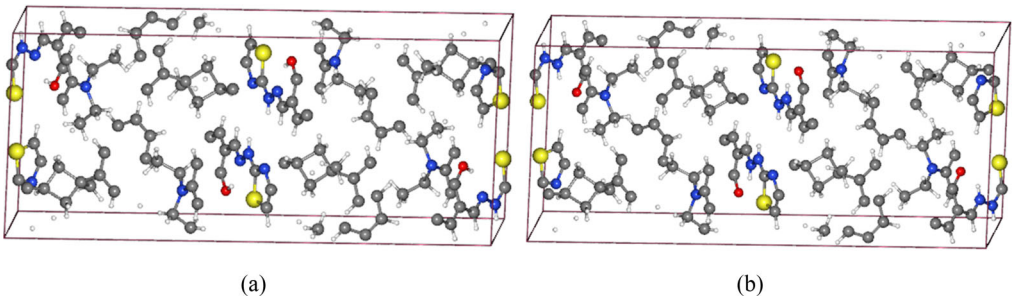

Figure 7. Representation of crystalline a) enol-imine b) keto-amine forms by atoms in the unit cell.

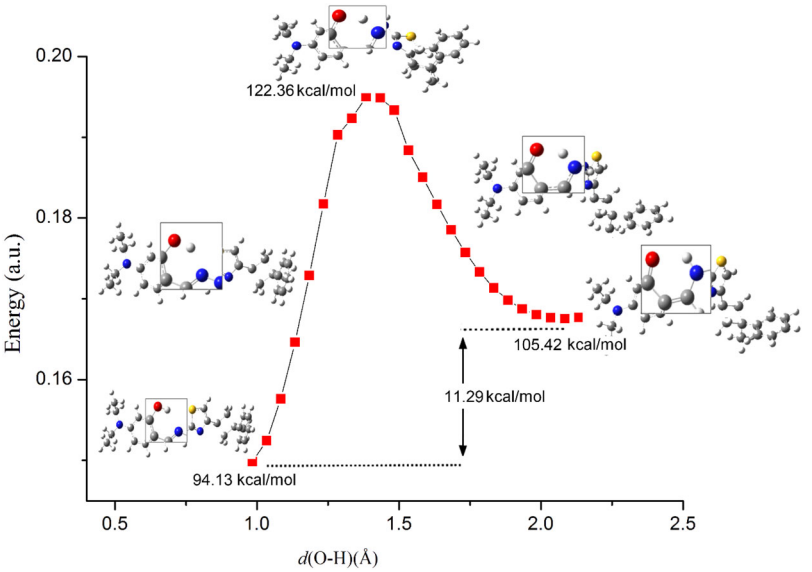

Figure 8. The energies of the title compound against the energy minimized conformer versus the O1–H1 bond distance during proton transfer.

structures was calculated as being 11.29 kcal/mol and the potential barrier was calculated as being 122.36 kcal/mol (Figure 8).

Variations between bond distance and total energy are shown in Figure 9. Referring to Figure 9, it is seen that the bond lengths change to adopt the enol-imine form. However, during stable enol-imine tautomer formation, the bond lengths of C21–O1 [1.355 (3) Å] and C15–C16 [1.439(4) Å] convert into single bond and C15–N3 [1.282 (3) Å] convert into double bond.

3.3. IR spectroscopy

The experimental FT-IR spectra of the compound were measured by Mattson 1000 Fourier transform FT-IR spectrophotometer in the 4000–400 cm^{-1} region. The calculated scaled Harmonic-vibration frequencies of the compound were performed by the B3LYP/6-31G(d,p) method. The title compound molecule has 177 normal vibrational modes of 61 atoms and under C1 point group symmetry. Figure 10 shows the graph of the calculated and experimental fundamental vibration frequencies versus the % transmittance values of the title compound. The inconsistency between the experimental and calculated frequencies is that the experimental results are carried out in the solid phase and the theoretical calculations in the gas phase, which do not take account the intermolecular interactions.[42]

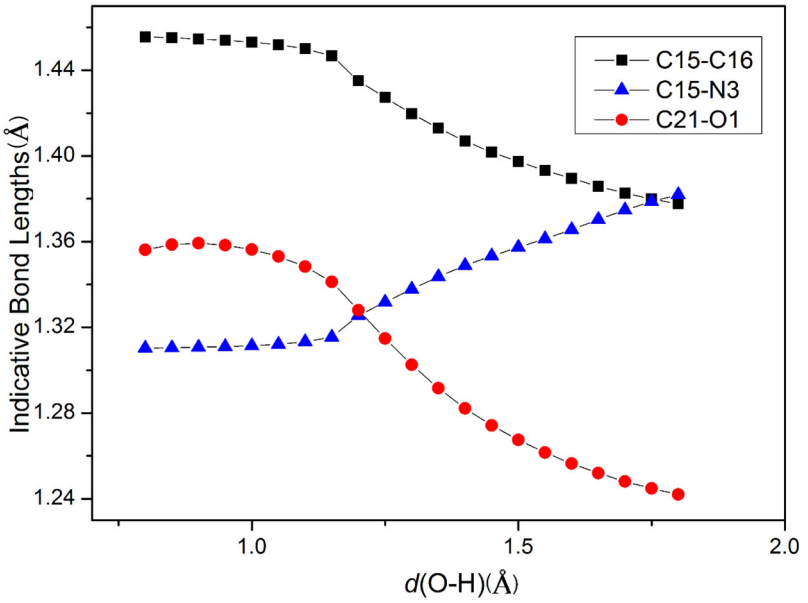

Figure 9. Variations of the indicative bond lengths versus the scan coordinate d (O–H).

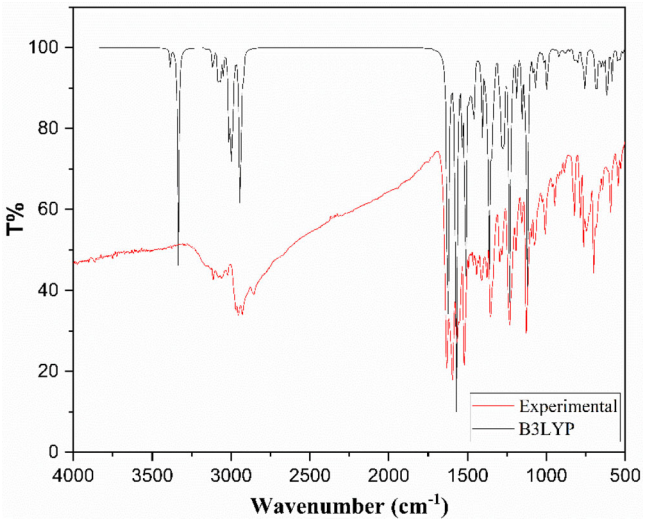

Figure 10. Simulated experimental and B3LYP levels FT-IR spectra of the title compound.

The O–H group vibrations show significant changes in FT-IR spectra due to intermolecular interactions. Hydroxyl stretching vibrations are generally observed in the region around 3500 cm^{-1}.[43] Similarly, in our case the stretching vibration of the O–H group was not observed in the FT-IR spectra because it was used in the intramolecular bond.[44] However, this band was calculated at 3356 cm^{-1}. The O–H in-plane and out–of–plane bending vibrations were observed as a medium-strength band at 1282 cm^{-1} and 638 cm^{-1}, respectively and theoretically calculated at 1214 and 687 cm^{-1} which is in good agreement with the experimental spectrum. The stretching vibration frequency of the N–H group with intermolecular bonding has been observed between 3200–2400 cm^{-1}.[45] In our study, the vibration frequency was observed at 2973 cm^{-1}

experimentally and theoretically calculated as 3406 cm^{-1}. In the literature, this frequency has been calculated at 3418 cm^{-1}.[45]

In the IR spectrum, characteristic C-H vibrational frequencies in heteroaromatic compounds are observed in the range of 3100–3000 cm^{-1}.[46,47] Aromatic C-H vibration frequencies in benzene and phenol rings have been experimentally observed at 3118–3040 cm^{-1} and the literature value are in agreement with 3042 cm^{-1}.[45] Theoretical vibration frequency was obtained in the range of 3155–2918 cm^{-1}. The C = N bond vibrations of the carbazone and thiazole groups were experimentally observed at 1634 and 1596 cm^{-1} while these peaks were calculated at 1608 and 1569 cm^{-1} for B3LYP, respectively. The C-H (aliphatic) bond vibration was experimentally observed at 2973–2858 cm^{-1} and 2978–2927 cm^{-1} in the literature.[48] Some other vibration modes and PED (Potential Energy Distribution) contributions are given in Table 4.

3.4. NMR spectroscopy

Experimental ^{1}H-NMR and ^{13}C-NMR spectra were measured using a Varian Mercury spectrometer (Figure 11) and theorical calculations performed on the optimized structure using the GIAO (Gauge-Independent Atomic Orbital)[49,50] and the B3LYP/6–31G(d, p) method. Due to the electronegative properties of the N1 and S1 atoms, the C14 atom has a greater chemical shift value than the others, at 168.6 ppm and the carbon atom peaks of the benzene ring were observed between 124.7 and 148.3 ppm. In addition, due to the very high shielding effect of methyl groups, all values are $\leq$3 ppm,[51] observed and calculated chemical shifts for hydrogen atoms are very low. In our study, the chemical shift values of the protons attached to the C7, C23 and C25 atoms were lower than the other peaks. There peaks were observed at 1.5–1.18 ppm and showed a good agreement with the calculated chemical shift values in the range of 1.92–0.79 ppm. The formation of intermolecular or intramolecular hydrogen bonds results in lower chemical shift values of proton signals of the OH group.[52,53] In our study, the proton peak of OH group was observed at 10.7 ppm and the chemical shift value observed in the literature was less than 12.0 ppm.[54] The proton peaks of amine NH and CH in the thiazole ring were observed as 6.05 and 7.20–7.10 ppm, respectively. Table 5 shows a good agreement between the experimental and theoretical chemical shift results of the compound.

Due to its ability to explain the location and strength of molecular deshielding and shielding areas in the outer field, the ICSS contour has been used as a powerful method to study the aromaticity of many compounds.[55–58] Information about the aromaticity of the molecule can be provided by inducing a ring current by an external magnetic field in π-electronic conjugation. Figure 12(a,b) shows the zz component of ICSS (ICSSzz) based on the response behavior of the molecule to the applied external magnetic field.

As shown in the figure, the orange isosurface (positive Z-component shielding value) shielding areas and the blue isosurface (negative Z-component shielding value) occurring in the outer region of the molecule shows the deshielding area. In Figure 12(c), the shielding area completely covers the area above and below the regions outside the part of the triazole and phenol ring in the molecule, which is the Z component of the magnetic shielding value since the direction of the external magnetic field $\vec{B}_0$ is parallel with the direction of the induced magnetic field caused by the spherical delocalized π-electrons. it is great.

Also, the deshielding field occurring in the outer region of the molecule is that the induced magnetic field in the molecule is parallel to the applied outer magnetic field $\vec{B}_0$, and thus increases $\vec{B}_0$ in this region. It is clearly seen in Figure 12(c) that some of the triazole and phenol ring are also coated with blue isosurface. This is because the σ-electrons included in the bonds in the rings form a noticeable locally induced ring current.[59] The graph in Figure 12(d) shows that the maximum Z component of the magnetic shielding value occurs about 3.1 Bohr above the plane of the title compound.

Table 4. Comparison of the observed and calculated vibrational spectra of title compound.

I_{IR} Intensity (kcal/mol)	Experimental FT-IR (cm^{-1})	Scaled FT-IR B3LYP/6 311G(d.p) (cm^{-1})	Assignments with PED (%) ($\geq$10%)
21.06	3120	3406	νNH (99)
295.89		3356	νOH (99)
1.72	3118	3155	νCH (99)
7.84		3116	νCH (99)
18.31		3111	νCH (97)
25.00		3080	νCH (23) + νCH (48) + νCH (21)
39.39		3069	νCH (34) + νCH (17) + νCH (34) +νCH (13)
11.25		3062	νCH (27) + νCH (37) + νCH (25)
0.32		3052	νCH (22) + νCH (38) + νCH (30)
8.58	3040	3049	νCH (18) + νCH (13) + νCH (14) + νCH (27) + νCH (28)
13.90		3048	νCH (98)
67.48		3014	νCH (16) + νCH (55) + νCH (10)
7.77		3013	νCH (55) + νCH (12) + νCH (18)
32.71		3006	νCH (41) + νCH (55)
49.22		2998	νCH (47) + νCH (43)
26.24		2998	νCH (46) + νCH (42)
30.12		2998	νCH (54) + νCH(37)
14.59		2991	νCH (54) + νCH (42)
49.82		2988	νCH (61) + νCH (12) + νCH (25)
7.68		2974	νCH (13) + νCH (47) + νCH (19)
6.40		2971	νCH (20) + νCH (49) + νCH (18)
7.16		2950	νCH (50) + νCH (38)
34.76		2943	νCH (37) + νCH (50)
36.23	2973	2941	νCH (96)
79.14		2939	νCH (32) + νCH (18) + νCH (14) + νCH (30)
14.78	2858	2938	νCH (95)
51.49		2931	νCH (18) + νCH (12) + νCH (14) +νCH (17) + νCH (12)
21.98		2930	νCH (18) + νCH (10) + νCH (15) + νCH (23) + νCH (12) + νCH(20)
16.97		2929	νCH (20) + νCH (23)
27.02		2918	νCH (37) + νCH (30) + νCH (25)
700.47		1622	νCC (18) + νCC (22) + νCC (10)
13.60	1634	1608	νNC (57) + δHCC (12)
9.07		1597	νCC (21) + νCC (17) + δCCC (13)
1.61		1573	νCC (29) + νCC (29) + δCCC (14) +δHCC (10)
978.76	1596	1569	νNC (27) + νNC (27) + δHNC (19)
67.68		1532	νCC (22) + νCC (21) + τHCCC (16)
63.05		1520	νCC (69) + νCC (13)
442.30		1507	νNC (16) + δHCC (12) + δHCC (10) + δCCC(11)
14.02		1481	δHCC (18) + δHCC (16) + δHCC (17) + δHCC (15)
6.40		1476	δHCN (10) + τHCNC (10) + τHCNC (16) + τHCNC(12)
56.03		1468	νCC (11) + τHCNC (13) + τHCNC (10)
48.38		1460	δHCN(15) + τHCCN (14)
6.91		1457	νCH(15) + τHCCN (17) + τHCCN (17) + τHCCN (14)
5.54		1456	δHCC(12)
2.14		1450	δHCC (12) +δHCH (38)+τHCCC (15)
0.01		1448	δHCH (23) +τHCCN (21)
0.80		1448	δHCC (15) +τHCCC (35)+τHCCC (16)
2.38		1447	δHCH (13) +τHCCN (21)
21.39		1444	τHCNC(10) +τHCNC (10)+τHCNC (12)
0.70		1431	δHCC (11) +τHCCC (11)+τHCCC (11) +τHCCC (14) +τHCCC (14)
6.37		1429	νCC (13) + νCC (13)+δHCC (10) +δHCC (22) +δHCC (12)
19.21		1411	νNC (23) +δHNC (20)+δHCC (14)
84.31		1398	νNC (14) + τHCCC (16)
26.97		1372	νCH (14) +δHCC (24)+δHCH (27)
14.10		1369	νCH(34) +δHCC (21)
2.33		1365	δHCC (45) +δHCH (45)
138.29		1363	τAHCCC(20) +δHCC (12)
168.23		1351	δHCN (21) +δHCN (24)
93.45		1349	νNC (11) + νCC (10)+ νCH(30)
75.23		1334	δHCC (15) +δHCN (15)+δHCN (16)
31.84		1327	νCC (17)

(*continued*)

Table 4. Continued.

I_{IR} Intensity (kcal/mol)	Experimental FT-IR (cm^{-1})	Scaled FT-IR B3LYP/6 311G(d.p) (cm^{-1})	Assignments with PED (%) ($\geq$10%)
8.60		1324	δHNC (22) +δHCC (23)
0.14		1310	νCC (10) + δHCC (22) + δHCC(12) + δHCC (23)
63.28	1131	1291	νOC (14) + δHCN (20) + δHCN (15)
1.32		1286	νCC (15) + νCC (32)
16.01		1279	νCC (19)
78.02		1278	νNC (11) + νNC (17)
146.69		1267	νNC (11) + δHCC (16)
16.46		1249	νNC (28) + δHCC (11) + δHCC (14)
1.29		1231	δHCC (16) + δHCC (23)
300.25		1229	δHNC (13)
108.03		1226	νCC (13) + νOC (10) + δHCC (13) + δHCC (26)
33.68		1218	τHCCC(42)
15.51		1214	νCC (10) + δHNC (11) + δHCC (20)
0.41		1193	δHCC (14) + δHCC (11) + δHCC (13)
41.56		1181	νNC (18) + νNC (18)
2.70		1175	δHCC (16) + δHCC (14)
0.81		1162	νCC (11) + δHCC (19) + δHCC (18) + δHCC (19) + δHCC (18)
52.00		1150	νCC (12) + νNN (13) + δHCC(10) +δHCC (21)
0.05		1141	δHCC (18) + δHCC (38) + δHCC (18)
12.14		1137	δHCC (19) + τHCCC (14)
26.56		1133	νCC (12) + δHCC (31) + τHCCC (10)
0.99		1129	νNN (22)
341.40		1117	νNN (13) + δHCC (12)
16.56		1077	δHCC (19) + δHCC (10)
5.96		1071	δHCC (25) + δCCC (11)
4.10		1065	νCC (18) + νCC (16) + δHCC (12)
27.82		1061	δHCC (25) +HCCN (10)
11.78		1051	νCC (13) + νCC (12) + δHCC (14)
9.86		1014	νCC (22) + νCC (28)
23.77		998	νNC (18) + νCC (25)
38.50		991	νNC (11) + νNC (14)+ νCC (15) + νCC(20)
1.65		983	νCC (12) + νCC (25) + γCCCC (10)
0.85		977	δCCC (27) + δCCC (20) + δNNC (20)
0.29		956	HCCC(16) + τHCCC (22) + τHCCC (18) + τCCCC) + τCCCC (10)
2.38		941	νCC (18) +δCCC (20)+δCCC(15)
0.01		933	HCCC(27) +τHCCC (26)+τHCCC (21)+ τHCCC (18)
3.48		923	δHCC (12) +δCCC (17)
9.51		917	HCCC(17) +τHCNN (67)
1.93		898	νCC (26) + νCC (32)+δHCC (12)
0.11		891	νCC (14)
0.82		890	τHCCC(20) +τHCCC (23)+τHCCC (17)
0.63		889	τHCCC(17) +τHCCC (52)+τHCNN (20)
7.96		879	νCC (16) + νCC (10)+ νCC (14)
1.86		865	δCCC (12)
2.63		850	νCC (17) +δNNC (10)
0.18		827	τHCCC(23) +τHCCC (24)+τHCCC (22) +τHCCC(24)
11.69		822	νSC (35) +δSCC (11)+δCCC (10)
1.80		818	τHCCC(11) +τHCCC (10)+τHCCC (12)
5.03		815	νCC (14)
21.88		802	τHCCN(69)
7.23		768	δHCC (13) +HCNC (20)+τHCNC (20) +τHCCN (17)
10.39		765	δHCC (13) +δHCC (17)+τHCNC (17) +τHCNC (22)
23.76		759	τHCCC(40)
15.37		758	νSC (17) +δCCC (14)+τHCCC (19)
17.58		750	τHCCC(16) +τHCCC (17)+τHCCC (19) +τCCCC(17) +γCCCC (12)
2.32		700	νCC (10) +δCCC (11)
14.67	701	679	τHCSC (42)

ν: stretching, δ: in-plane bending, γ: out-of-plane bending, τ: torsion.

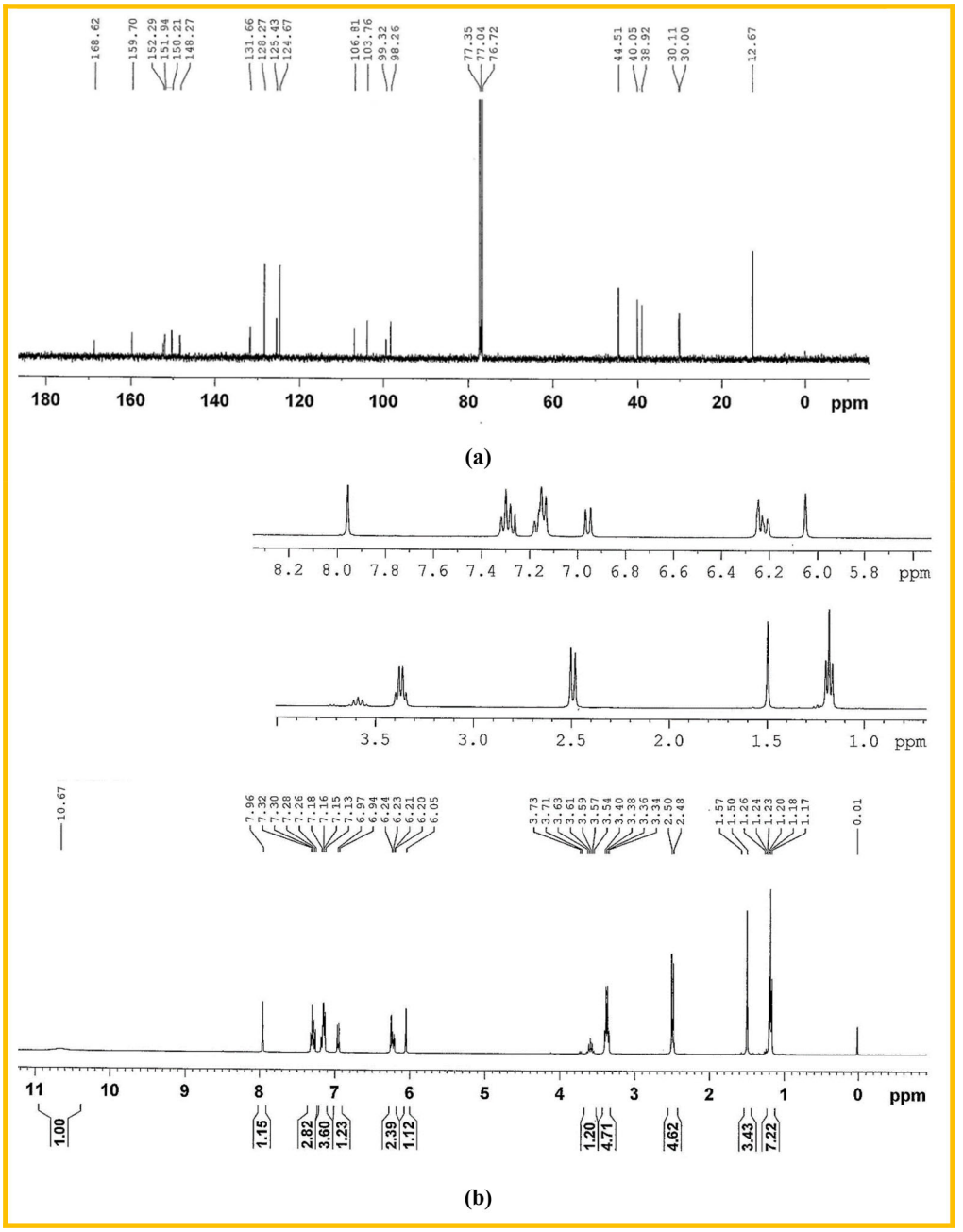

Figure 11. Experimental (a) ^{1}H NMR (b) ^{13}C NMR spectrum of target compound.

3.5. Electronic absorption spectra and frontier molecular orbitals

In o–hydroxy Schiff–based compounds, enol-imine structure shows the presence of a peak at <400 nm in the UV–visible spectrum, while the keto-amine structure shows peak at >400 nm[60] in polar and nonpolar solvents. Experimentally, the electronic absorption spectra of the title compound in chloroform solvent show two peaks supporting the enol-imine form at 380.8 (log $\varepsilon = 4.79$) and 265.3 (log $\varepsilon = 4.19$) nm. These values are like those in the literature.[61–63] Due to the

Table 5. Theoretical and experimental ^{13}C and ^{1}H isotropic chemical shifts.

Atom	Experimental (ppm) Chloroform phase	B3LYP/6–31G(d,p) (ppm) Chloroform phase
C1	124.7	118.9
C2	128.3	121.5
C3	124.7	118.9
C4	128.3	121.6
C5	125.4	118.8
C6	148.3	146.7
C7	30.0	31.8
C8	24.6	42
C9	44.5	42.4
C10	16.5	32.8
C11	38.92	37.2
C12	159.7	149.5
C13	106.8	101.8
C14	168.6	160.1
C15	150.2	135.9
C16	99.8	101.6
C17	131.7	126.7
C18	103.8	97.4
C19	151.9	141.7
C20	98.3	92.2
C21	152.3	152.6
C22	40.05	44.4
C23	12.67	12.6
C24	30.1	44.2
C25	10.1	13.4
H (OH)	10.67	8.73
H (–NH–)	7.20-7.10	7.01
H (=CH-S)	6.05	5.66
CH (N = CH–)	7.96	7.09
CH (aromatics)	6.96–6.20	7.2–5.8
CH_3 (cyclobutane)	1.50	1.92-1.27
CH_2 (cyclobutane)	2.49	2.66–2.18
CH (cyclobutane)	3.56	3.58
CH_2 (aniline group)	3.36	3.43–3.18
CH_3 (aniline group)	1.18	1.46–0.79

C = N functional group of Schiff bases, they are expected to make n–π^* and π–π^* transitions. The peaks of the π–π^* transitions are known to shift to the higher energy region with increased solvent polarity.[64] It can be said that the higher wavelength value from these transitions belongs to the n–π^* transition and the lower wavelength values belong to the π–π^* transition. In the UV spectra of the title compound, the bands appearing at 265.3 nm represent π–π^* transitions, while the band at 380.8 nm represents n–π^* transitions (Figure 13).

The electronic absorption spectra were calculated in the time-independent TD–DFT method on the structure optimized with the B3LYP/6–31G(d, p) base set. TD–DFT calculation in chloroform solvent was performed using the PCM model. The calculated major two absorption bands were found to be 369.4 and 229.5 nm and the oscillator strengths are 1.2671 and 0.1078, respectively. These transitions of the compound are given in Table 6.

The activity of an inhibitor is closely related to Frontier molecular orbitals (HOMO and LUMO). Frontier molecular orbitals play an important role in UV–Vis spectra, chemical reactions, electrical and optical properties.[65,66] Figure 14(a) shows the distribution and energy levels of LUMO + 4 [C14 (%19), C13 (%17), C12 (%11), C21 (%9), N2 (%8)], LUMO + 3 [C17 (%26), C20 (%20), C18 (%15), C21 (%15), C14 (%4)], LUMO [C15 (%24), N3 (%19), C19 (%11), C17 (%9), C17 (%6)], HOMO [N4 (%16), N2 (%13), C16 (%13), N3 (%9), C13 (%9)], HOMO–1 [N4 (%18), C13 (%18), C12 (%10), C20 (%9), N2 (%7)] and HOMO–5 [S1 (%17), N1 (%12), C12 (%12), C17 (%9), N4 (%7)] of occupied and unoccupied molecular orbitals. In addition, contributions from atomic orbitals; for LUMO + 4, LUMO + 3, LUMO, HOMO, HOMO – 1 and

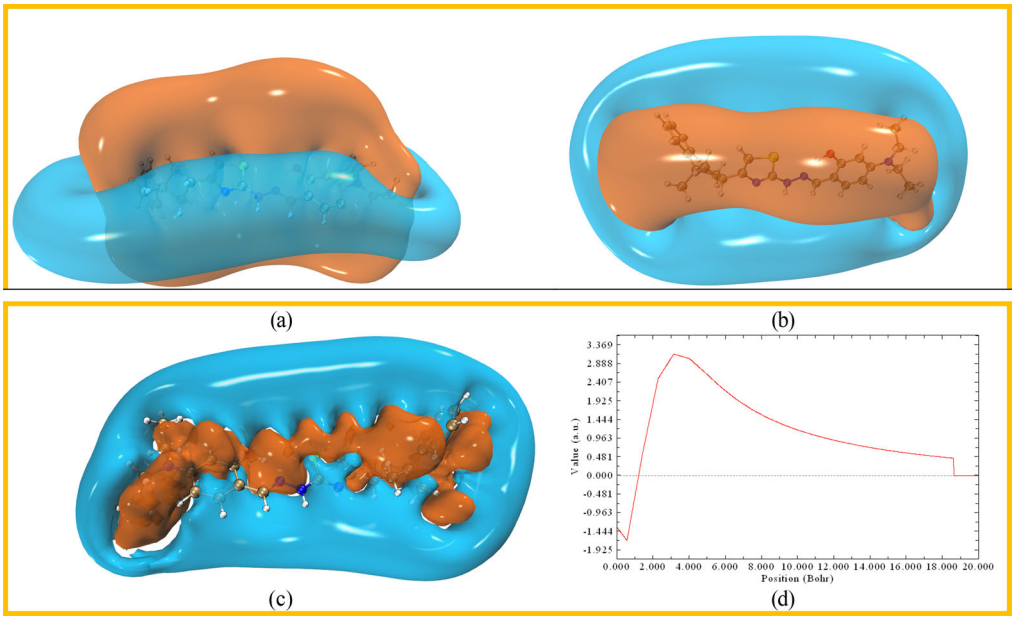

Figure 12. Shielding surfaces at 0.02 ppm are in blue, and deshielding surfaces at 0.02 ppm are in orange.

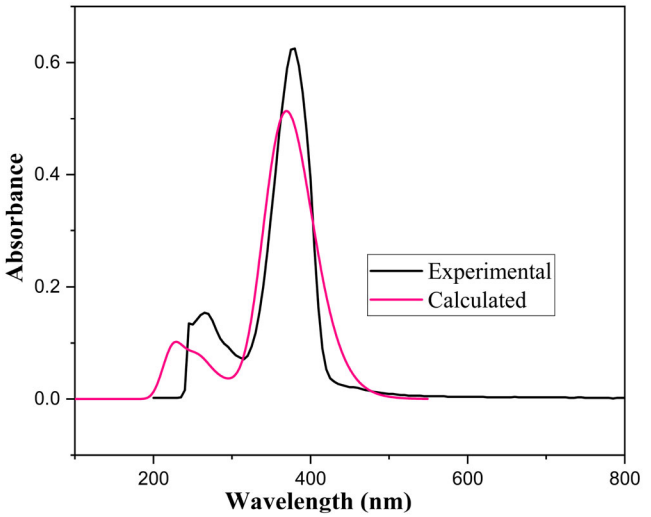

Figure 13. Experimental and theoretical UV–Vis spectra of the title compound. frag.1:phenol ring; frag.2: N2 and N3 atoms; frag.3: thiazole ring; frag.4: N4 atom; DOS: density-of-states; TDOS: total density-of-states; PDOS partial density-of-states; OPDOS: overlap density-of-states.

Table 6. Experimental and calculated absorption wavelength (λ_{max}), excitation energies (*E*), oscillator strength (*f*), assignment and excited state of the title compound.

		Wavelength (nm)			
Major excited state and **contribs.**	E (eV)	Experimental	Calculated	Oscillator strength (f)	Assignment
Excited state-1 H→L (%98)	3.359	380.8	369.4	1.2671	n→π*
Excited state-2 H–5→L (%53) H–1→L + 3 (%27) H–1→L + 4 (%14)	5.403	265.3	229.5	0.1078	π→π*

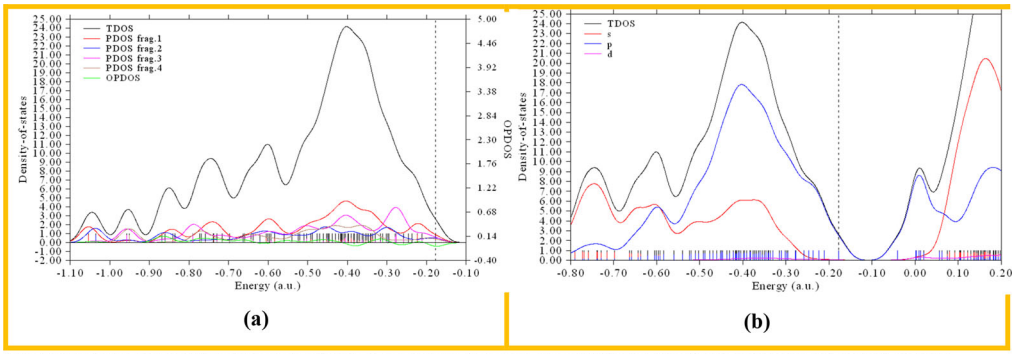

frag.1:phenol ring; frag.2:N2 and N3 atoms; frag.3: thiazole ring; frag.4:N4 atom; DOS: density-of-states; TDOS:total density-of-states. PDOS partial density-of-states; OPDOS: overlap density-of-states

Figure 14. Plot TDOS, PDOS and OPDOS for specific fragments.

HOMO – 5 energy levels (Figure 15) are calculated as s (1.7%) + p (95.4) + d (2.9%), s (2.3%) + p (95.2) + d (2.5%), s (0.86%) + p (96.7) + d (2.4%), s (2.2%) + p (95.7) + d (2.0%), s (3.2%) + p (94.9) + d (1.9%) and s (3.4%) + p (95.0) + d (1.6%), respectively (Figure 14(b)).

The energy difference value between HOMO and LUMO orbitals is 1.61 eV, and this large energy gap indicates that the title compound is very stable.

3.6. Reactivity descriptors

Global reactivity descriptors

E_{HOMO} is associated with direct ionization potential energy (IP) and E_{LUMO} is associated with electron affinity (EA) and is given as equation follows.

$$\mathrm{IP} = -\ E_{\mathrm{HOMO}} \quad [1]$$

$$\mathrm{EA}_{=} - E_{\mathrm{LUMO}} \quad [2]$$

Likewise, electronegativity (χ), absolute hardness (η), chemical potential (μ) and global hardness (S) indexes are given by the following equations.[67–69]

$$\chi = \mathrm{IP} + \mathrm{EA}/2 \quad [3]$$

$$\eta = \ \mathrm{IP} - \mathrm{EA}/2 \quad [4]$$

$$\mu = -\chi \quad [5]$$

$$\mathrm{S} = \eta/2 \quad [6]$$

These parameters were used to obtain the electron fraction (δ) values of the enol-imine and keto-amine structures of the title molecule. δ, refers to the number of electrons that transfer from the inhibitor to the metal surface and the following equation.[70]

$$\delta = \frac{\chi_B - \chi_A}{2(\eta_B + \eta_A)}$$

In the equation χ_B and η_B are the electronegativity and absolute hardness of the metal atoms respectively, while χ_A and η_A are the values of the title compound. If $\delta < 3.6$, the corrosion inhibition effect increases with the increase of electrons given on the metal surface.[71] In this study, the corrosion effect on Cu and Fe metal atoms was investigated and calculations were made by taking $\chi_{Cu} = 4.48\mathrm{eV/mol}$,[72] $\eta_{Cu} = 0\mathrm{eV/mol}$,[73] $\chi_{Fe} = 7\mathrm{eV/mol}$ and $\eta_{Fe} = 0\mathrm{eV/mol}$.[74] According to the data in Table 7, both forms of the title compound were found to have higher

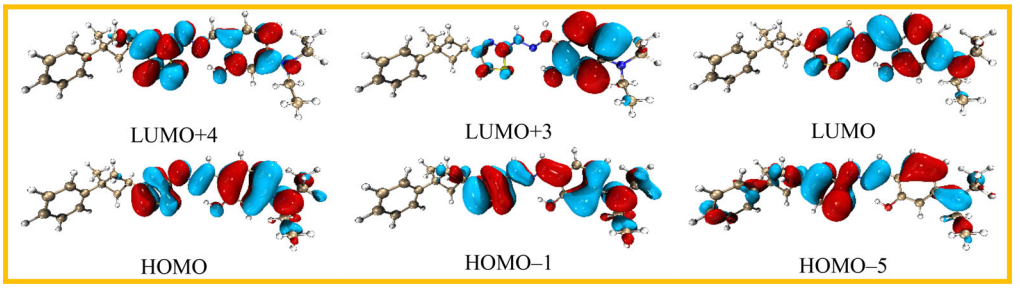

Figure 15. Molecular orbital surfaces given in parentheses for the HOMO, HOMO-1, HOMO-5, LUMO, LUMO + 3 and LUMO + 4 of the title compound.

anticorrosion effect for the Fe metal atom than the Cu metal, while the enol-imine form had higher value for both Fe and Cu metals. These findings show that enol-imine form will give the best result as a corrosion inhibitor for Fe and Cu metals than keto-amine form.

Local reactivity descriptors

Fukui functions of the title compound were obtained from Hirshfeld charges by B3LYP/6-31G (d, p) method. Fukui functions give information about active regions (electrophilic or nucleophilic reactions) in a molecule. Fukui functions are given below.[75]

$$f^{+}(r) = \rho_{N+1}(r) - \rho_{N}(r), \text{ for nucleophilic attack} \quad [6]$$

$$f^{-}(r) = \rho_{N}(r) - \rho_{N-1}(r), \text{ for electrophilic attack} \quad [7]$$

where $\rho_N(r)$, $\rho_{N+1}(r)$ and $\rho_{N-1}(r)$ denotes the electronic population on atom k for the N(Neutral), $N+1$(anionic) and N-1(cationic) electron systems, respectively. The $f^{+}(r)$ nucleophilic and $f^{-}(r)$ are functions that determine susceptibility to nucleophilic and electrophilic attack, respectively. Another method used to explain chemical reactivity is to calculate local softness (S_k^+ and S_k^-) indices. These functions are related to condensed Fukui functions and are given by the following equations.[76]

$$S_k^+ = Sf_k^+ \quad [8]$$

$$S_k^- = Sf_k^- \quad [9]$$

where + and – signs are describe nucleophilic and electrophilic attacks, respectively. Fukui functions are local reactivity identifiers and are used only to compare reactive atomic centers within the same molecule, while local softness identifiers (S_k^+ *and* S_k^+) are used to compare reactivity between similar atoms of different molecules.[76] In addition, relative electrophilicity ($S_k^+(r)/S_k^-(r)$) and relative nucleophilicity ($S_k^-(r)/S_k^+(r)$) indices are defined for the two tautomer structures of the title compound and these were used to predict the reactive sites of the two structures. The values of the Fukui functions for the nucleophilic and electrophilic attack of the two inhibitors (enol-imine and keto-amine) are given in Table 8 and the nucleophilic and electrophilic regions on the molecule are shown in Figure 16. In Figure 16, nucleophilic and electrophilic attack regions are mostly localized on the Thiazole and phenol rings and N2/N3 atoms. For the nucleophilic attack, the most reactive region of the enol-imine and keto-amine form is on the C15 atom, for the electrophilic attack, it is on the N2 atom of the enol-imine form and on the O1 atom of the keto-amine form. In Table 9, the average values of Fukui functions and local softness indices of both tautomer structures are given for the Thiazole and phenol rings and N2/N3/C15 group atoms. According to Fukui functions, the most nucleophilic and electrophilic regions in the enol-imine form are on the N2/N3/C15 atom group. The most electrophilic region

Table 7. Inhibition values of two tautomers.

Inhibitor	$\delta-$ Fe	$\delta-$ Cu
Enol-imine	1.0985	0.4252
Keto-amine	0.9944	0.3210

Table 8. Selected reactivity descriptors as Fukui functions, local softnesses using Hirshfeld atomic charges of two tautomers.

Enol-imine							Keto-amine					
Atom	f_k^-	f_k^+	S^-	S^+	S^+/S^-	S^-/S^+	f_k^-	f_k^+	S^-	S^+	S^+/S^-	S^-/S^+
O1	0.026	0.0299	0.1099	0.1264	1.1504	0.8693	0.1009	0.0633	0.4077	0.2558	0.6275	1.5936
N1	0.0473	0.0418	0.1998	0.1767	0.8844	1.1307	0.0203	0.0226	0.082	0.0911	1.1114	0.8998
N2	0.0625	0.0115	0.264	0.0487	0.1846	5.4157	0.0206	0.0048	0.0834	0.0194	0.2325	4.3007
N3	0.0322	0.0732	0.1357	0.309	2.2768	0.4392	0.0198	0.0553	0.0799	0.2233	2.7953	0.3577
N4	0.0614	0.0235	0.2592	0.0993	0.383	2.6111	0.0374	0.0275	0.1509	0.1112	0.7374	1.3561
S1	0.0249	0.0172	0.105	0.0725	0.6903	1.4486	0.0336	0.0147	0.1358	0.0593	0.4364	2.2913
C1	−4E-4	0.0055	−0.0017	0.0233	−13.6997	−0.073	0.0087	0.0052	0.035	0.0209	0.5963	1.677
C2	0.0055	0.0098	0.0232	0.0416	1.7912	0.5583	0.0107	0.0108	0.0433	0.0437	1.0071	0.9929
C3	0.0089	0.0183	0.0375	0.0773	2.0603	0.4854	0.0224	0.0079	0.0904	0.0321	0.3548	2.8182
C4	0.0061	0.0118	0.0256	0.0498	1.9431	0.5146	0.013	0.0095	0.0523	0.0385	0.737	1.3568
C5	0	0.0047	1E-4	0.02	174.214	0.0057	0.0072	0.0067	0.0293	0.0273	0.9314	1.0736
C6	−0.0047	0.0053	−0.0197	0.0226	−1.1472	−0.8717	0.0103	−9E-4	0.0416	−0.0035	−0.0832	−12.021
C7	0.0031	0.0036	0.0129	0.0154	1.1903	0.8402	0.0046	0.0027	0.0186	0.011	0.59	1.6951
C8	0.0036	0.0033	0.0152	0.014	0.9192	1.0879	0.0027	0.0016	0.0109	0.0064	0.5895	1.6965
C9	0.0045	0.0025	0.0188	0.0107	0.5684	1.7592	0.0063	0.002	0.0255	0.0082	0.3212	3.1136
C10	2E-4	6E-4	7E-4	0.0024	3.3235	0.3009	0.0029	0.001	0.0119	0.0042	0.3535	2.8289
C11	0.0026	0.003	0.0108	0.0125	1.1607	0.8615	0.0045	0.0023	0.0183	0.0092	0.5017	1.9931
C12	0.0332	0.022	0.1402	0.093	0.663	1.5082	0.0249	0.0138	0.1006	0.0559	0.5556	1.8
C13	0.0609	0.0401	0.2573	0.1694	0.6584	1.5188	0.0369	0.0211	0.1492	0.0852	0.5708	1.7518
C14	0.0106	0.0266	0.0447	0.1124	2.5157	0.3975	0.0077	−0.0011	0.0312	−0.0044	−0.1421	−7.0397
C15	0.0261	0.0919	0.1102	0.3878	3.5194	0.2841	0.0253	0.1144	0.1024	0.462	4.5134	0.2216
C16	0.0457	0.0136	0.1928	0.0573	0.2969	3.3678	0.0139	0.0192	0.0559	0.0777	1.3883	0.7203
C17	0.0254	0.044	0.1071	0.1859	1.736	0.5761	0.0345	0.057	0.1394	0.23	1.6502	0.606
C18	0.0475	0.0267	0.2004	0.1129	0.5634	1.7749	0.0359	0.0512	0.1449	0.2069	1.4278	0.7004
C19	0.0271	0.0503	0.1145	0.2123	1.8541	0.5393	0.0233	0.0515	0.094	0.2081	2.2142	0.4516
C20	0.0262	0.0236	0.1107	0.0997	0.9004	1.1106	0.093	0.0314	0.3754	0.1266	0.3374	2.9641
C21	0.0199	0.027	0.084	0.1138	1.3558	0.7376	0.0272	0.0371	0.1097	0.1496	1.3645	0.7329
C22	0.0097	0.0061	0.0409	0.026	0.634	1.5773	0.0063	0.0076	0.0256	0.0308	1.2028	0.8314
C23	0.0114	0.0067	0.048	0.0284	0.5917	1.6899	0.0086	0.0084	0.0346	0.0337	0.9757	1.025
C24	0.0094	0.0063	0.0395	0.0264	0.6691	1.4945	0.0083	0.0073	0.0334	0.0294	0.8808	1.1353
C25	0.0114	0.0069	0.048	0.029	0.6031	1.658	0.0098	0.0082	0.0395	0.033	0.8369	1.1949

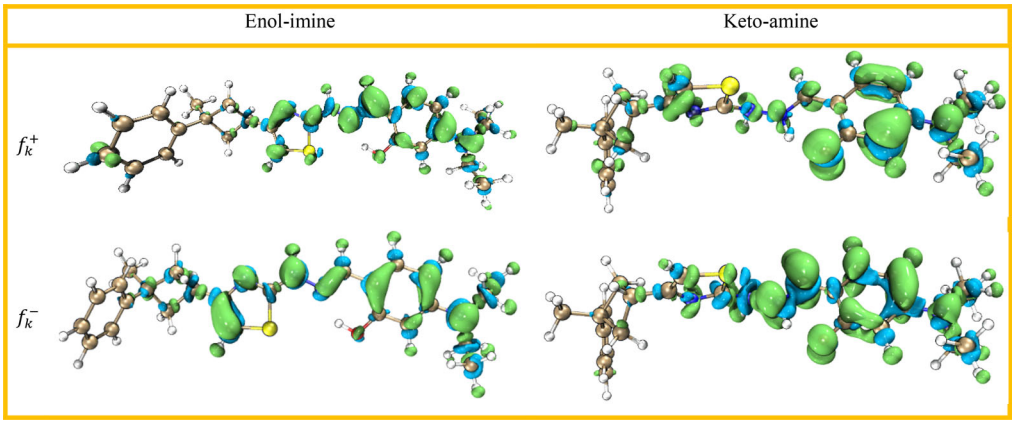

Figure 16. Map representation of Fukui functions on two tautomers. In the map, green and blue isosurface correspond to positive and negative region of f_k^+ and f_k^-, respectively.

Table 9. Fukui functions and local softness average values of some atoms in the enol-imine and keto-amine forms.

Enol-imine			
	Thiazole ring	Phenol ring	N2/N3/C15 atoms
f_k^-	0.03538	0.03111	0.0399
f_k^+	0.02954	0.03073	0.058867
S_k^-	0.1494	0.13134	0.16997
S_k^+	0.1248	0.12976	0.2485
Keto-amine			
f_k^-	0.02468	0.04696	0.0219
f_k^+	0.01422	0.04439	0.05817
S_k^-	0.09976	0.18957	0.08857
S_k^+	0.05742	0.17924	0.2349

in the keto-amine form is on the phenol ring, while the most nucleophilic region is on the N2/N3/C15 atom group. When local softness indices $S_k^+(r)$ and $S_k^-(r)$ values were used to compare the two tautomer structures, the thiazole ring and N2/N3/C15 atom group are the most nucleophilic region in the enol-imine form, while the phenol ring is the most electrophilic region in the keto-amine form. Therefore, the thiazole ring and the N2/N3/C15 atom group of the enol-imine form will be more reactive than the keto-amine form in a nucleophilic reaction. Likewise, the phenol ring of the keto-amine form will be more reactive in the electrophilic reaction than the enol-imine form.

4. Conclusion

Theoretical studies have been conducted using the B3LYP level with 6-31 G(d, p) to determine the reactive behavior of the newly synthesized Schiff base-containing 5-diethylamino-2-{[4-(3-methyl-3-phenyl-cyclobutyl)-thiazol-2-yl]-hydrazonomethyl}-phenol compound, which may be a corrosion inhibitor. In addition, a study was carried out using quantum chemical calculations to determine the corrosion inhibition activity behavior on Cu and Fe metals using the global chemical parameters of tautomer structures. With the calculated HOMO and LUMO energies of the compound, some quantum chemical parameters such as electron affinity (EA), ionization potential (IP), electronegativity (χ), absolute hardness (η), chemical potential (μ), absolute softness (S) were calculated. Using these parameters, the electron transfer fraction (δ) coefficient, which determines the charge transfer of the whole compound from the inhibitor to the metal, was calculated. Tautomer's nucleophilic and electrophilic attack sites were determined by calculating the chemical constants, quantum chemical parameters and local selectivity indices and Fukui functions of the two tautomer structures of the title compound.

Disclosure statement

No potential conflict of interest was reported by the authors.

Funding

Computing resources used in this work were provided by the National Center for High Performance Computing of Turkey (UHeM) under grant number 5005172018.

ORCID

Tuncay Karakurt http://orcid.org/0000-0001-6944-9883
Muharrem Dinçer http://orcid.org/0000-0003-3960-9991

Alaaddin Cukurovali http://orcid.org/0000-0002-8297-2350
Ibrahim Yilmaz http://orcid.org/0000-0002-9447-3065

References

1. H. Kargar, A. A. Ardakani, M. N. Tahir, M. Ashfaq, and K. S. Munawar, "Synthesis, Spectral Characterization, Crystal Structure Determination and Antimicrobial Activity of Ni (II), Cu (II) and Zn (II) Complexes with the Schiff Base Ligand Derived from 3, 5-Dibromosalicylaldehyde," *Journal of Molecular Structure* 1229, (2021) : 129842.
2. H. Kargar, V. Torabi, A. Akbari, R. Behjatmanesh-Ardakani, A. Sahraei, and M. N. Tahir, "Pd (II) and Ni (II) Complexes Containing an Asymmetric Schiff Base Ligand: Synthesis, X-Ray Crystal Structure, Spectroscopic Investigations and Computational Studies," *Journal of Molecular Structure* 1205, (2020) : 127642.
3. H. Kargar, V. Torabi, A. Akbari, R. Behjatmanesh-Ardakani, A. Sahraei, and M. N. Tahir, "Synthesis, Crystal Structure, Spectroscopic Investigations, and Computational Studies of Ni (II) and Pd (II) Complexes with Asymmetric Tetradentate NOON Schiff Base Ligand," *Structural Chemistry* 30, no. 6 (2019) : 2289–99.
4. H. Kargar, M. Fallah-Mehrjardi, R. Behjatmanesh-Ardakani, V. Torabi, K. S. Munawar, M. Ashfaq, and M. N. Tahir, "Sonication-Assisted Synthesis of New Schiff Bases Derived from 3-Ethoxysalicylaldehyde: Crystal Structure Determination, Hirshfeld Surface Analysis, Theoretical Calculations and Spectroscopic Studies," *Journal of Molecular Structure* 1243 (2021) : 130782.
5. K. S. Munawar, S. Ali, M. N. Tahir, N. Khalid, Q. Abbas, I. Z. Qureshi, S. Hussain, and M. Ashfaq, "Synthesis, Spectroscopic Characterization, X-Ray Crystal Structure, Antimicrobial, DNA-Binding, Alkaline Phosphatase and Insulin-Mimetic Studies of Oxidovanadium (IV) Complexes of Azomethine Precursors," *Journal of Coordination Chemistry* 73, no. 16 (2020) : 2275–300.
6. Z. H. Chohan, M. Arif, and M. Sarfraz, "Metal-Based Antibacterial and Antifungal Amino Acid Derived Schiff Bases: their Synthesis, Characterization and in Vitro Biological Activity," *Applied Organometallic Chemistry* 21, no. 4 (2007) : 294–302.
7. V. Tsapkov, V. Prisacar, S. Buracheva, D. Lazakovich, and A. Gulya, "Synthesis and Antimicrobial Activity of Sulfazine-Containing Copper (II) Coordination Compounds with Substituted Salicylaldehydebenzoylhydrazones," *Pharmaceutical Chemistry Journal* 42, no. 9 (2008) : 523–6.
8. A. Rauf, A. Shah, K. S. Munawar, S. Ali, M. N. Tahir, M. Javed, and A. M. Khan, "Synthesis, Physicochemical Elucidation, Biological Screening and Molecular Docking Studies of a Schiff Base and Its Metal (II) Complexes," *Arabian Journal of Chemistry* 13, no. 1 (2020) : 1130–41.
9. J.R. Davis, Corrosion: Understanding the Basics (Materials Park, Ohio: ASM International, 2000).
10. C. Vargel, Corrosion of Aluminium, 2nd Ed., (Amsterdam: Elsevier, 2020).
11. E. Torsner, "Solving Corrosion Problems in Biofuels Industry, Corrosion Engineering," *Science and Technology* 45, no. 1 (2010) : 42–8.
12. D. K. Verma, R. Aslam, J. Aslam, M. Quraishi, E. E. Ebenso, and C. Verma, "Computational Modeling: Theoretical Predictive Tools for Designing of Potential Organic Corrosion Inhibitors," *Journal of Molecular Structure* 1236 (2021) : 130294.
13. N. P. Kolenchin, V. Kuskov, and P. Shadrina, "New Technologies of Anodizing Components of Oil and Gas Industry Equipment Made of Aluminum Alloys," *Applied Mechanics and Materials* 770 (2015) : 121–5.
14. G. Elewady, I. El-Said, and A. Fouda, "Anion Surfactants as Corrosion Inhibitors for Aluminum Dissolution in HCl Solutions," *International Journal of Electrochemical Science* 3, no. 2 (2008) : 177–90.
15. M. Finšgar, and J. Jackson, "Application of Corrosion Inhibitors for Steels in Acidic Media for the Oil and Gas Industry: A Review," *Corrosion Science* 86 (2014) : 17–41.
16. N. Nnaji, N. Nwaji, J. Mack, and T. Nyokong, "Ball-Type Phthalocyanines and Reduced Graphene Oxide Nanoparticles as Separate and Combined Corrosion Inhibitors of Aluminium in HCl," *Journal of Molecular Structure* 1236 (2021) : 130279.
17. N. Abdelshafi, "Electrochemical and Molecular Dynamic Investigation of Some New Pyrimidine Derivatives as Corrosion Inhibitors for Aluminium in Acid Medium," *Protection of Metals and Physical Chemistry of Surfaces* 56, no. 5 (2020) : 1066–80.
18. B. E.-D. M. El-Gendy, S. T. Atwa, A. A. Ahmed, and Y. Ali, "Synthesis and Characterization of Carbon Steel Corrosion Inhibitors Based on 4, 5, 6, 7-Tetrahydrobenzo [b] Thiophene Scaffold," *Protection of Metals and Physical Chemistry of Surfaces* 55, no. 1 (2019) : 179–86.
19. K. C. Emregül, and M. Hayvalí, "Studies on the Effect of a Newly Synthesized Schiff Base Compound from Phenazone and Vanillin on the Corrosion of Steel in 2 M HCl," *Corrosion Science* 48, no. 4 (2006) : 797–812.

20. C. T. Zeyrek, B. Boyacioglu, and H. Ünver, "Density Functional Modelling Studies of Chloride-Substituted Schiff Bases as Corrosion Inhibitors: Optimized Geometries, Atomic Charges, Solvent and Non-Linear Optical Effects," *Protection of Metals and Physical Chemistry of Surfaces* 53, no. 1 (2017) : 159–76.
21. E. E. Ebenso, D. A. Isabirye, and N. O. Eddy, "Adsorption and Quantum Chemical Studies on the Inhibition Potentials of Some Thiosemicarbazides for the Corrosion of Mild Steel in Acidic Medium," *International Journal of Molecular Sciences* 11, no. 6 (2010) : 2473–98.
22. A. D. Becke, "Density-Functional Thermochemistry. III. The Role of Exact Exchange," *The Journal of Chemical Physics* 98, no. 7 (1993) : 5648–52.
23. C. Lee, W. Yang, and R. G. Parr, "Development of the Colle-Salvetti Correlation-Energy Formula into a Functional of the Electron Density," *Physical Review B Condensed Matter* 37, no. 2 (1988) : 785–9.
24. P. Hohenberg, and W. Kohn, "Inhomogeneous Electron Gas," *Physical Review* 136, no. 3B (1964) : B864–B871.
25. M. Frisch, G. Trucks, H.B. Schlegel, G. Scuseria, M. Robb, J. Cheeseman, G. Scalmani, V. Barone, B. Mennucci, G. Petersson, Gaussian 09, revision a. 02 (Wallingford, CT: Gaussian, Inc., 2009).
26. T. Keith, J. Millam, R. Dennington, GaussView, version 5 (Shawnee Mission KS: Semichem Inc., 2009).
27. E. Cances, B. Mennucci, and J. Tomasi, "A New Integral Equation Formalism for the Polarizable Continuum Model: Theoretical Background and Applications to Isotropic and Anisotropic Dielectrics," *The Journal of Chemical Physics* 107, no. 8 (1997) : 3032–41.
28. M. J. Dewar, E. G. Zoebisch, E. F. Healy, and J. J. Stewart, "Development and Use of Quantum Mechanical Molecular Models. 76. AM1: A New General Purpose Quantum Mechanical Molecular Model," *Journal of the American Chemical Society* 107, no. 13 (1985) : 3902–9.
29. T. Lu, and F. Chen, "Multiwfn: A Multifunctional Wavefunction Analyzer," *Journal of Computational Chemistry* 33, no. 5 (2012) : 580–92.
30. J. P. Perdew, K. Burke, and M. Ernzerhof, "Generalized Gradient Approximation Made Simple," *Physical Review Letters* 77, no. 18 (1996): 3865–8.
31. P. Giannozzi, S. Baroni, N. Bonini, M. Calandra, R. Car, C. Cavazzoni, D. Ceresoli, G. L. Chiarotti, M. Cococcioni, I. Dabo, et al. "Quantum Espresso: A Modular and Open-Source Software Project for Quantum Simulations of Materials," *Journal of Physics. Condensed Matter* 21, no. 39 (2009): 395502.
32. G. M. Sheldrick, " SHELXT - Integrated Space-Group and Crystal-Structure Determination ," *Acta Crystallographica Section A* 71, no. Pt 1 (2015) : 3–8.
33. G. M. Sheldrick, "Crystal Structure Refinement with Shelxl," *Acta Crystallographica Section C: Structural Chemistry* 71, no. 1 (2015) : 3–8.
34. O. V. Dolomanov, L. J. Bourhis, R. J. Gildea, J. A. Howard, and H. Puschmann, "OLEX2: A Complete Structure Solution, Refinement and Analysis Program," *Journal of Applied Crystallography* 42, no. 2 (2009) : 339–41.
35. T. Karakurt, A. Cukurovali, and İ. Kani, "Structure of 2-(2-(Anthracen-9-Ylmethylene) Hydrazinyl)-4-(3-Methyl-3-Phenylcyclobutyl) Thiazole by Combined X-Ray Crystallographic and Molecular Modelling Studies," *Molecular Physics* 118, no. 15 (2020) : e1718224.
36. T. Karakurt, M. Dinçer, and A. Cukurovali, "Syntheses, Spectral Characterization, Single Crystal X-Ray Diffraction and Computational in Gas and Solid Phases Studies on Chloro-Acetic Acid N′-(2-Hydroxy-Naphthalen-1-Ylmethylene)-N-[4-(3-Methyl-3-Phenyl-Cyclobutyl)-Thiazol-2-yl]-Hydrazide," *SN Applied Sciences* 2, no. 4 (2020) : 1–16.
37. T. Karakurt, A. Cukurovali, N. T. Subasi, A. Onaran, A. Ece, S. Eker, and I. Kani, "Experimental and Theoretical Studies on Tautomeric Structures of a Newly Synthesized 2, 2′(Hydrazine-1, 2-Diylidenebis (Propan-1-yl-1-Ylidene)) Diphenol," *Chemical Physics Letters* 693 (2018) : 132–45.
38. A. Filarowski, A. Koll, and T. Głowiak, "Structure and Hydrogen Bonding in Ortho-Hydroxy Ketimines," *Journal of Molecular Structure* 644, no. 1–3 (2003) : 187–95.
39. M. Kabak, A. Elmali, Y. Elerman, and I. Svoboda, "Conformations and Structures of N, N'-Bis (2-Methoxybenzylidene)-1, 3-Diamino-Propanol and N, N'-Bis (3-Methoxybenzylidene)-1, 3-Diamino-Propanol," *Zeitschrift Für Naturforschung B* 58, no. 11 (2003) : 1141–6.
40. T. Karakurt, "Investigation of the Molecular Structure of 4-(3-methyl-3-phenylcyclobutyl)-2-[2-(3-methylbenzylidene)hydrazinyl]thiazole in the gas and solid phases," *Acta Crystallographica Section C, Structural Chemistry* 74, no. Pt 11 (2018): 1502–8.
41. F. H. Allen, "The Geometry of Small Rings. VI. Geometry and Bonding in Cyclobutane and Cyclobutene," *Acta Crystallographica Section B Structural Science* 40, no. 1 (1984) : 64–72.
42. T. Karakurt, M. Dinçer, A. Çukurovalı, and İ. Yılmaz, "Ab Initio and Semi-Empirical Computational Studies on 5-Hydroxy-4-Methyl-5, 6-di-Pyridin-2-yl-4, 5-Dihydro-2H," *Journal of Molecular Structure* 991, no. 1–3 (2011) : 186–201.

43. D. Sajan, H. Joe, V. Jayakumar, and J. Zaleski, "Structural and Electronic Contributions to Hyperpolarizability in Methyl p-Hydroxy Benzoate," *Journal of Molecular Structure* 785, no. 1–3 (2006) : 43–53.
44. A. Cukurovali, and T. Karakurt, "Synthesis, Spectroscopic, X-Ray Diffraction and Tautomeric Properties of 5-(Diethylamino)-2-((2-(5-(3-Methyl-3-Phenylcyclobutyl)-6H-1, 3, 4-Thiadiazin-2yl) Hydrazono) Methyl) Phenol: A Combined Experimental and Theoretical Study," *Journal of Molecular Structure* 1189 (2019) : 328–37.
45. T. Karakurt, A. Cukurovali, N. T. Subasi, and I. Kani, "Molecular Structure and Computational Studies on 2-((2-(4-(3-(2, 5-Dimethylphenyl)-3-Methylcyclobutyl) Thiazol-2-yl) Hydrazono) Methyl) Phenol Monomer and Dimer by DFT Calculations," *Journal of Molecular Structure* 1125 (2016) : 433–42.
46. V. K. Rastogi, M. A. Palafox, R. P. Tanwar, and L. Mittal, *Spectrochimica Acta A* 58, no. 9 (2002): 1987-2004.
47. M. Silverstein, G.C. Basseler, C. Morill, Spectrometric Identification of Organic compounds (New York: Wiley, 1981).
48. T. Karakurt, M. Dinçer, I. Yılmaz, and A. Čukurovalı, "1-{(2E)-2-[(Aminocarbonothioyl) Hydrazono]-2-(3-Mesityl-3-Methylcyclobutyl) Ethyl} Pyrrolidine-2, 5-Dione," *Acta Crystallographica Section E Structure Reports Online* 59, no. 12 (2003) : o1997–o1999.
49. R. Ditchfield, "Molecular Orbital Theory of Magnetic Shielding and Magnetic Susceptibility," *The Journal of Chemical Physics* 56, no. 11 (1972) : 5688–91.
50. K. Wolinski, J. F. Hinton, and P. Pulay, "Efficient Implementation of the Gauge-Independent Atomic Orbital Method for NMR Chemical Shift Calculations," *Journal of the American Chemical Society* 112, no. 23 (1990) : 8251–60.
51. F.A. Cotton, G. Wilkinson, C.A. Murillo, M. Bochmann, R. Grimes, Advanced Inorganic Chemistry (New York: Wiley, 1988).
52. S. R. Salman, S. H. Shawkat, and G. M. Al-Obaidi, "Tautomerism in Chlorinated O-Hydroxyschiff Bases: Effect of Chlorine Atom Substitution," *Spectroscopy Letters* 22, no. 10 (1989) : 1265–73.
53. M. Yıldız, Z. Kılıç, and T. Hökelek, "Intramolecular Hydrogen Bonding and Tautomerism in Schiff Bases. Part I. Structure of 1, 8-di [N-2-Oxyphenyl-Salicylidene]-3, 6-Dioxaoctane," *Journal of Molecular Structure.* 441, no. 1 (1998) : 1–10.
54. A. Ramamoorthy, C. Wu, and S. Opella, "Magnitudes and Orientations of the Principal Elements of the 1H Chemical Shift, 1H− 15N Dipolar Coupling, and 15N Chemical Shift Interaction Tensors in 15Nε1-Tryptophan and 15Nπ-Histidine Side Chains Determined by Three-Dimensional Solid-State NMR Spectroscopy of Polycrystalline Samples," *Journal of the American Chemical Society* 119, no. 43 (1997) : 10479–86.
55. S. Klod, and E. Kleinpeter, "Ab Initio Calculation of the Anisotropy Effect of Multiple Bonds and the Ring Current Effect of Arenes—Application in Conformational and Configurational Analysis," *Journal of the Chemical Society, Perkin Transactions* 2, no. 10 (2001) : 1893–8.
56. E. Kleinpeter, and A. Koch, "Identification of Benzenoid and Quinonoid Structures by through-Space NMR Shieldings (TSNMRS)," *The Journal of Physical Chemistry A* 114, no. 18 (2010) : 5928–31.
57. E. Kleinpeter, S. Klod, and A. Koch, "Endohedral and External Through-Space Shieldings of the Fullerenes C50, C60, c60(-6), c70, and c70(-6)-Visualization of (Anti)Aromaticity and their Effects on the Chemical Shifts of Encapsulated Nuclei," *The Journal of Organic Chemistry* 73, no. 4 (2008) : 1498–507.
58. M. Baranac-Stojanovic, and E. Kleinpeter, "Quantification of the Aromaticity of 2-alkylidenethiazolines subjected to push-pull activity ," *The Journal of Organic Chemistry* 76, no. 10 (2011) : 3861–71.
59. T. Lu and F. Chen, "Multiwfn: A Multifunctional Wavefunction Analyzer," *Journal of Computational Chemistry*, 33 (2012): 580–592.
60. S. R. Salman, and F. S. Kamounah, "Mass Spectral Study of Tautomerism in Some 1-Hydroxy-2-Naphthaldehyde Schiff Bases," *Spectroscopy Letters* 35, no. 3 (2002) : 327–35.
61. B. Chattopadhyay, S. Basu, P. Chakraborty, S. K. Choudhuri, A. K. Mukherjee, and M. Mukherjee, "Synthesis, Spectroscopic Characterization, X-Ray Powder Structure Analysis, DFT Study and in Vitro Anticancer Activity of N-(2-Methoxyphenyl)-3-Methoxysalicylaldimine," *Journal of Molecular Structure* 932, no. 1–3 (2009) : 90–6.
62. Z. Cai-Rong, L. Zi-Jiang, C. Yu-Hong, C. Hong-Shan, W. You-Zhi, and Y. Li-Hua, "DFT and TDDFT Study on Organic Dye Sensitizers D5, DST and DSS for Solar Cells," *Journal of Molecular Structure: THEOCHEM* 899, no. 1–3 (2009) : 86–93.
63. F. F. Jian, P. S. Zhao, Z. S. Bai, and L. Zhang, "Quantum Chemical Calculation Studies on 4-Phenyl-1-(Propan-2-Ylidene) Thiosemicarbazide," *Structural Chemistry* 16, no. 6 (2005) : 635–9.
64. Z. Hayvali, M. Hayvali, Z. Kiliç, T. Hökelek, and E. Weber, "New Benzo-15-Crown-5 Ethers Featuring Salicylic Schiff Base Substitutions–Synthesis, Complexes and Structural Study," *Journal of Inclusion Phenomena and Macrocyclic Chemistry* 45, no. 3/4 (2003) : 285–94.

65. J. Fleming, Frontier Orbitals and Organic Chemical Reactions (London: John Wiley, 1976).
66. T. Karakurt, M. Dinçer, A. Cetin, and M. Sekerci, "Molecular Structure and Vibrational Bands and Chemical Shift Assignments of 4-allyl-5-(2-hydroxyphenyl)-2,4-dihydro-3H-1,2,4-triazole-3-thione by DFT and Ab Initio HF Calculations," *Spectrochimica Acta Part A, Molecular and Biomolecular Spectroscopy* 77, no. 1 (2010) : 189–98.
67. R. G. Parr, R. A. Donnelly, M. Levy, and W. E. Palke, "Electronegativity: The Density Functional Viewpoint," *The Journal of Chemical Physics* 68, no. 8 (1978) : 3801–7.
68. R. G. Parr, and R. G. Pearson, "Absolute Hardness: companion Parameter to Absolute Electronegativity," *Journal of the American Chemical Society* 105, no. 26 (1983) : 7512–6.
69. W. Yang, and R. G. Parr, "Hardness, Softness, and the Fukui Function in the Electronic Theory of Metals and Catalysis," *Proceedings of the National Academy of Sciences of the United States of America* 82, no. 20 (1985) : 6723–6.
70. K. O. Sulaiman, and A. T. Onawole, "Quantum Chemical Evaluation of the Corrosion Inhibition of Novel Aromatic Hydrazide Derivatives on Mild Steel in Hydrochloric Acid," *Computational and Theoretical Chemistry* 1093, (2016) : 73–80.
71. I. Lukovits, E. Kalman, and F. Zucchi, "Corrosion Inhibitors—Correlation between Electronic Structure and Efficiency," *Corrosion* 57, no. 1 (2001) : 3–8.
72. R. G. Pearson, "Absolute Electronegativity and Hardness: Application to Inorganic Chemistry," *Inorganic Chemistry* 27, no. 4 (1988) : 734–40.
73. S. Martinez, "Inhibitory Mechanism of Mimosa Tannin Using Molecular Modeling and Substitutional Adsorption Isotherms," *Materials Chemistry and Physics.* 77, no. 1 (2003) : 97–102.
74. G. Gece, and S. Bilgiç, "A Theoretical Study of Some Hydroxamic Acids as Corrosion Inhibitors for Carbon Steel," *Corrosion Science* 52, no. 10 (2010) : 3304–8.
75. R. G. Parr and W. Yang, Density Functional Theory of Atoms and Molecules (New York, NY: Oxford University Press, 1989).
76. H. Wang, X. Wang, H. Wang, L. Wang, and A. Liu, "DFT Study of New Bipyrazole Derivatives and Their Potential Activity as Corrosion Inhibitors," *Journal of Molecular Modeling* 13, no. 1 (2007) : 147–53.